

# Combined colorimetric and gravimetric CMUT sensor for detection of benzyl methyl ketone

**Mølgaard, Mathias J.G.; Laustsen, Milan; Jakobsen, Mogens H.; Andresen, Thomas L.; Thomsen, Erik V.**

*Published in:*
Sensors and Actuators B: Chemical

*Link to article, DOI:*
10.1016/j.snb.2018.07.136

*Publication date:*
2018

*Document Version*
Peer reviewed version

# Combined Colorimetric and Gravimetric CMUT Sensor for Detection of Benzyl Methyl Ketone

Mathias J. G. Mølgaard, Milan Laustsen, Mogens H. Jakobsen, Thomas L. Andresen, Erik V. Thomsen

*Department of Micro and Nanotechnology, Technical University of Denmark, DK-2800 Kgs. Lyngby, Denmark*

**Abstract**

The detection of benzyl methyl ketone (BMK) is of interest as it is a common precursor for the synthesis of (meth)amphetamine. Resonant gravimetric sensors can be used to detect the mass and hereby the concentration of a gas while colorimetric arrays typically have exceptional selectivities to a target analyte. We present a sensor system consisting of a Capacitive Micromachined Ultrasonic Transducer (CMUT) and a colorimetric array for detection of BMK. The CMUT is used as a resonant gravimetric gas sensor where the resonance frequency shift due to mass loading of the plate. A single Local Oxidation of Silicon (LOCOS) step was used to define the cavities which were sealed with a $Si_3N_4$ plate with a thickness of 100 nm, resulting in a resonance frequency of 38.8 MHz and a mass sensitivity of 28.3 $\frac{\text{zg}}{\text{Hz}\cdot\mu\text{m}^2}$ or $8.5 \times 10^3$ $\frac{\text{cm}^2}{\text{g}}$. This sensitivity is, to our knowledge, the best reported as compared with the state of the art of CMUTs. The CMUTs were functionalized with the same dyes used to fabricate the colorimetric arrays. While both the CMUT and the colorimetric array showed selectivity between BMK and acetone and water, the highest selectivity was achieved with the colorimetric array. Here the analyte BMK resulted in the only signal (color change), while acetone and water did not give any signal. Furthermore, the mass of the BMK was found as a function of time. Thus, the combination of a colorimetric array and a CMUT resulted in a sensor system with a selectivity between BMK, acetone and water and in addition a quantitative value for the mass.

*Preprint submitted to Sensors and Actuators B: Chemical* *August 7, 2018*

*Keywords:* CMUT, gravimetric, sensor, colorimetry

## 1. Introduction

Detection of illegal drug and explosive precursors is of interest for government agencies. Amphetamine and methamphetamine are recreational drugs and in most countries they are classified as controlled substances. A common synthesization route for these drugs involves the reductive amination of the illegal precursor molecule benzyl methyl ketone (BMK) [1]. Therefore, it is desirable to be able to detect BMK, especially in the gas phase.

The detection and identification of molecules in the gas phase can be done in a variety of ways, including: gas chromatography, infrared spectroscopy, nuclear magnetic resonance spectroscopy, mass spectrometry and by resonant gravimetric detection. Of these only the latter has the potential for miniaturization, low cost, low power consumption, and integration with integrated circuits, while still maintaining a high sensitivity and mass resolution [2]. Consequently, gravimetric sensors are strong candidates for mobile sensing systems or as distributed sensors. Examples of such sensors include: bulk acoustic wave (BAW) sensors: quartz crystal microbalances (QCMs) [3], and film bulk acoustic resonators (FBAR) [4], surface acoustic wave (SAW) sensors [5], micro- and nano-cantilevers/bridges [6], and capacitive micromachined ultrasonic transducers (CMUTs) [7]. The criteria for a good resonant gravimetric sensor for gas phase measurements are manyfold: high mass sensitivity, low limit of detection (LOD), high signal to noise ratio (SNR), and ease of functionalization. Based on these criteria the CMUT is an attractive candidate. The normalized CMUT mass sensitivity is high compared with the other sensor types, as will be shown in Section 5. Compared with the other gravimetric sensors the CMUT has a LOD per area which is among the lowest due to a combination of a low Allan deviation ($10^{-8}$ to $3 \cdot 10^{-8}$) and a relatively large surface area ($0.09\,\mathrm{mm}^2$ to $0.25\,\mathrm{mm}^2$) [2]. A single CMUT sensor is typically comprised of hundreds to thousands of CMUT cells connected electrically in parallel, lowering the overall

impedance and noise [7], while increasing the SNR. The ease of massive parallelism of the CMUT cells is contrasted by the other gravimetric sensor types that often are comprised of a single resonating structure.

CMUTs have previously been used for sensing applications. In 2007 Park *et al.* demonstrated the use of CMUTs as sensors by detecting water, isopropanol, acetone, and methanol [8]. The sarin stimulant molecule dimethyl methylphosphonate (DMMP) has been detected by CMUTs with a volume LOD of 50.5 pptv and a volume sensitivity of 34.5 pptv/Hz [7]. These results show that unprecedented sensitivities and LODs can be obtained using CMUTs as gravimetric sensors. CMUTs have also been used as biosensors, specifically as an immunosensor where the antigen antibody pair interacts in a highly selective reaction causing the resonance frequency to decrease [9]. Finally, CMUTs have also been used for environmental monitoring where the concentration of $CO_2$ has been measured [10] [11].

A functional layer is needed in order to make the gravimetric sensors selective towards a specific analyte. Functionalization is typically done by applying a thin coating on top of the resonator. Due to the closed and planar surface of the CMUT device several methods can be employed including: spin coating, drop coating, dip coating, and spray coating. One method of improving selectivity between multiple analytes in a gas has been to employ several CMUT elements each coated with a different functionalization layer [12]. A single chip with several CMUT elements can easily be fabricated, thus minimizing the footprint and complexity.

In this paper we combine a CMUT sensor with a colorimetric array to detect BMK. Doing so, we benefit from the selectivity between BMK, acetone and water offered by the colorimetric array and the sensitivity and quantitative output of the CMUT. Furthermore, having two independent sensor types combined provides the total sensor system with redundancy. The article is structured as follows: first the fabrication and characterization of the CMUT and colorimetric array is presented. Then the experimental setup is described, followed by the results in the form of the CMUT and colorimetric response. Finally a short

discussion and comparison of normalized sensitivities for different gravimetric resonators is given.

## 2. The Sensors

This section describes the fabrication and characterization of the CMUT and colorimetric chip.

### *2.1. CMUT*

#### *2.1.1. Fabrication*

The CMUT process flow can be seen in Figure 1. In step (1) a $SiO_2$ layer was grown on a low electrical resistivity Si wafer ($< 0.025\,\Omega$cm, <100>). A $Si_3N_4$ layer was deposited by LPCVD and subsequently patterned using UV lithography and a $H_3PO_4$ etch. In step (2) local oxidation of silicon (LOCOS) was performed using the patterned $Si_3N_4$ as the oxidation mask [13].

The cavities were, in step (3), sealed under vacuum by fusion bonding a layer of 100 nm $Si_3N_4$ on a double side polished Si handle wafer to the cavity wafer. Prior to the bonding process all wafer pairs were RCA cleaned to remove any particles. The pre-bonding process was performed in a wafer bonding machine (Süss Microtec, Substrate Bonder SB6 Gen2), with a piston pressure of 667 mbar at a temperature of 50 °C and a gas pressure of $5 \cdot 10^{-4}$ mbar. Subsequently, the pre-bonded wafer pairs were annealed in a furnace at a temperature of 1100 °C for 70 min. The bonding of $Si_3N_4$ to $SiO_2$ is discussed further in Section 5.

The top $Si_3N_4$ layer in step (3) was etched in a dry etch. Hereafter, in step (4), the Si handle wafer was etched in KOH (28 wt%, 80 °C), which was chosen due to the high etch selectivity between Si and $Si_3N_4$. The $Si_3N_4$ plate and the $Si_3N_4$ layer on the backside of the cavity (bottom) wafer acted as etch stop layers for the KOH etch of the Si handle wafer. Bottom electrode openings were etched in step (5) with a dry etch and finally the Al top electrode was deposited and patterned in step (6) using a $H_3PO_4 : H_2O$ (2:1) etch at room temperature.

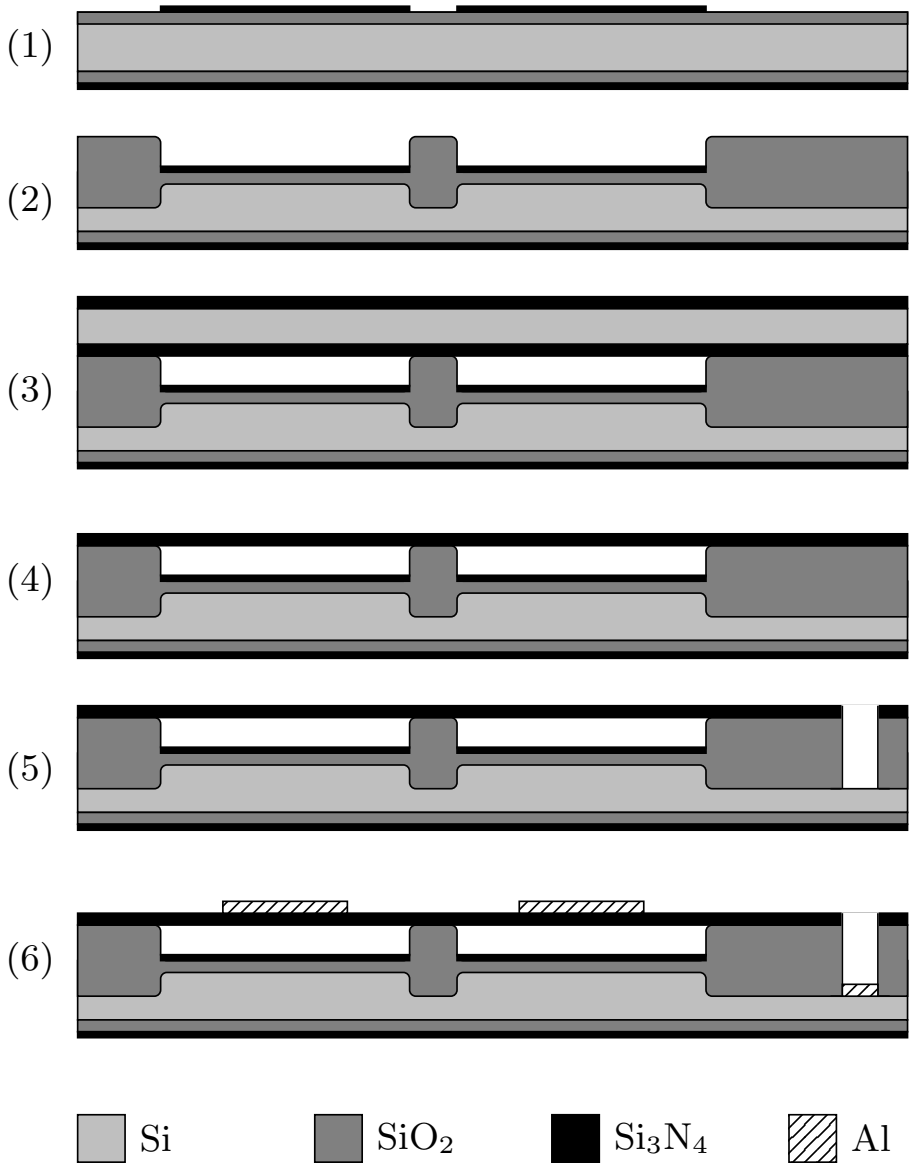


Figure 1: Process flow of the CMUT.

*2.1.2. Design and characterization*

The design parameters of the CMUT used for sensing is shown in Table 1. The resonance frequency was chosen to be around 40 MHz which is a compromise between obtaining a high sensitivity and staying below the upper frequency limit of the external electrical circuitry. The sensitivity was sought maximized by decreasing the mass of the plate which was achieved by having a thin plate (100 nm), which hereby uniquely determines the radius of the plate due to the fixed resonance frequency. Figure 2a) shows a top view optical microscope image of a CMUT element consisting of 100 individual cells. The dark circles are the individual CMUT cells, while the light-colored grid structure is the Al top electrode. The top electrode grid design is chosen to decrease the parasitic capacitance and the total mass of the plate and top electrode. The width of the individual grid lines of the Al top electrode is named $W$ and is defined in Figure 2a). A more narrow $W$ decreases the parasitic capacitance but decreasing $W$ increases the electrical resistance and ultimately $W$ is limited by the lithography system used. The choice of $W$ is therefore a trade-off between parasitic capacitance, sensitivity and electrical resistance. Figure 2b) shows a cross-sectional SEM image of a single CMUT cell. The figure shows the Bird's Beak formed by the growth of the $SiO_2$ at the edge of the cavity. Figure 2c) shows a zoom in which reveals that the $Si_3N_4$ edge is well below the bonding plane. The plate and metal layer bend upward, away from the substrate wafer. This could be due to the repulsion of negative electrical charges on the plate and substrate wafer from the electron beam of the SEM. However, since the Al top electrode and substrate wafer are grounded through the chip holder it is more likely that the bending of the plate is due to the biaxial tensile stress in the $Si_3N_4$ plate.

The elements used for sensing in this study consist of 1024 cells connected in parallel. The theoretical zero voltage capacitance of the CMUT cells is $C_{\mathrm{CMUT}} = 0.64\,\mathrm{pF}$ while the theoretical parasitic capacitance is $C_{\mathrm{parasitic}} = 4.62\,\mathrm{pF}$. Hence, the useful capacitance $C_{\mathrm{CMUT}}$ only makes up 12% of the total capacitance of the element, which in part is due to the wire bond pad which

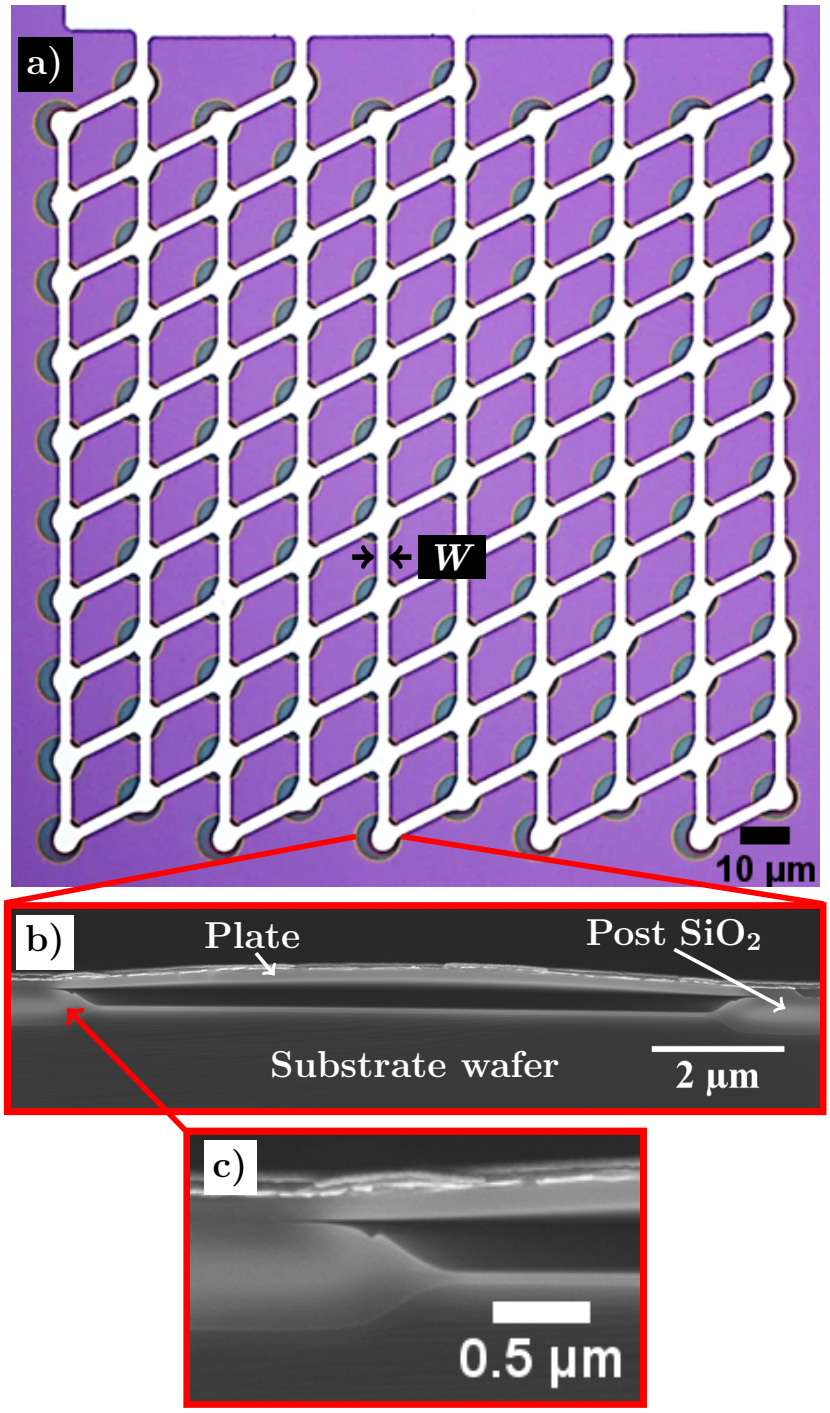


Figure 2: a) Top view of a CMUT element of 10 by 10 cells showing the grid pattern of the metal layer. b) Scanning electron microscope image of a cross-section of a single CMUT cell. c) Scanning electron microscope image zoomed in on the Bird's Beak structure and bonding interface.

Table 1: Properties of the fabricated CMUTs.

| **Parameter** | **Value** |
|---|---|
| Radius, $a$ | $5\,\mu$m |
| Plate thickness, $t$ | 100 nm |
| Metal thickness | 100 nm |
| Gap height | 255 nm |
| Metal line width, $W$ | $2.5\,\mu$m |
| Wire bond pad area | $(150\text{x}250)\,\mu\text{m}^2$ |
| LOCOS $Si_3N_4$ thickness | 50 nm |
| $Si_3N_4$ tensile stress | 1.3 GPa |
| Number of cells (sensing element) | 1024 |
| Resonance frequency, $f_0$ ($V_{\text{DC}} = \frac{2}{3}V_{\text{PI}}$) | 38.8 MHz |
| Pull-in voltage | 150 V |

accounts for 45% of the parasitic capacitance. In order to decrease this parasitic capacitance the area of the wire bond pad could be decreased. Another solution is to make a new design where the bond pad is raised above the plate by a polymer or dielectric material, thus effectively increasing the post height in this region, the downside being an additional lithography step. Figure 3 shows impedance spectra (Keysight, E4990A) of the CMUTs at three different DC voltages (Keithley, 2410) which demonstrates the spring softening effect. The resonance frequency and pull-in voltage is found from these spectra and was found to be $f_0 = 38.8\,\text{MHz}\,(\text{at}\,\frac{2}{3}V_{\text{PI}})$ and $V_{\text{PI}} = 150\,\text{V}$, respectively (see Table 1). The pull-in voltage has been determined from the impedance spectra by noting at which DC voltage the resonance peak disappears.

*2.1.3. Sensitivity*

Mass sensitivity is one of the key figures of merit of a gravimetric sensor. It can be calculated theoretically by approximating the CMUT as a 1-D linear harmonic oscillator and assuming that the mass added to the plate is much

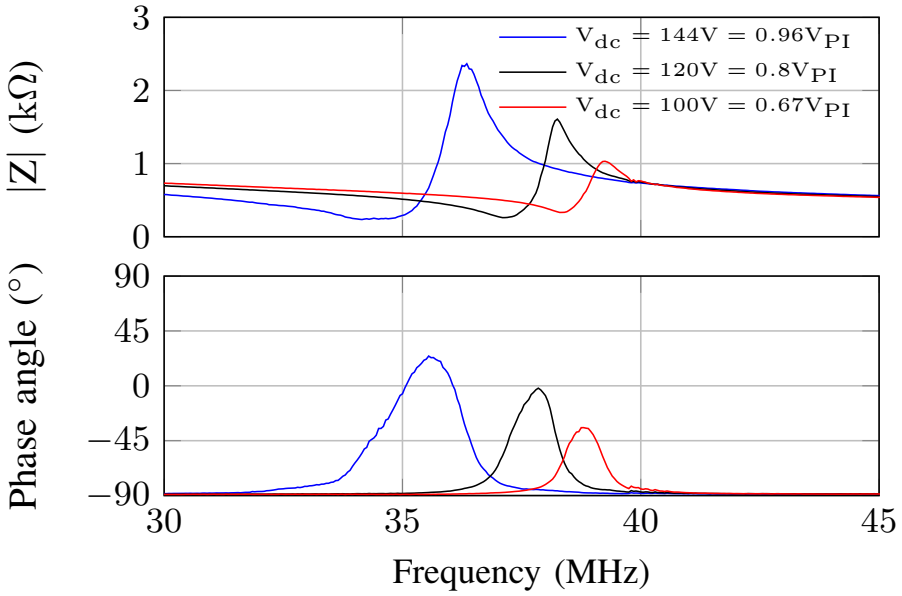


Figure 3: Impedance spectra of a CMUT device at three bias voltages.

smaller than the mass of the plate. The theoretical distributed mass sensitivity, $S_{\text{theoretical}}$, can then be expressed as [14]:

$$S_{\text{theoretical}} = \frac{\partial f_0}{\partial m} = -\frac{1}{2}\frac{f_0}{m_{\text{plate}}}, \tag{1}$$

where $f_0$ is the resonance frequency and $m_{\text{plate}}$ is the mass of the plate. The sensitivity is increased by having a plate with a high resonance frequency and a low mass. In this paper this is achieved by having a low plate mass of 46 pg due to a plate thickness of 100 nm and Al top electrode thickness of 100 nm, while maintaining a resonance frequency of 38.8 MHz. The theoretical sensitivity $S_{\text{theoretical}}$ for the CMUT device has been calculated using Equation 1: $S_{\text{theoretical}} = 0.45\,\frac{\text{Hz}}{\text{ag}}$. Table 2 shows both the theoretical sensitivity and the measured sensitivity of $S_{\text{measured}} = 0.24\,\frac{\text{Hz}}{\text{ag}}$. The measured sensitivity is found by determining the resonance frequency from impedance spectra and subsequently depositing a thin layer (11 nm) of Au on the CMUT element. Repeating the impedance measurement and deposition step, values of the resonance

Table 2: Table of the theoretical and measured sensitivity and limit of detection for the CMUT device.

| **Parameter** | **Value** |
|---|---|
| $S_{\text{theoretical}}$ | $0.45\,\frac{\text{Hz}}{\text{ag}}$ |
| $S_{\text{measured}}$ | $0.24\,\frac{\text{Hz}}{\text{ag}}$ |
| $S^{-1}_{\text{theoretical}}/A$ | $28.3\,\frac{\text{zg}}{\text{Hz}\cdot\mu\text{m}^2}$ |
| $S^{-1}_{\text{measured}}/A$ | $51.8\,\frac{\text{zg}}{\text{Hz}\cdot\mu\text{m}^2}$ |
| LOD($1\sigma$) | 2.0 ag |
| LOD/A($1\sigma$) | $25.8\,\frac{\text{zg}}{\mu\text{m}^2}$ |

frequency as a function of added mass is found. Figure 4 shows such a plot for the device. The amount of mass added to the plate is calculated from the area of the plate and by measuring the step height of the deposited Au using AFM. Finally, the measured sensitivity is obtained by fitting a linear expression to the data and extracting the slope. Table 2 shows theoretical and measured sensitivities. The ratio $S_{\text{measured}}/S_{\text{theoretical}} = 0.53$ shows that the measured sensitivity is worse than the predicted theoretical value. This can be due to an overestimation of the added Au mass or a violation of the assumption for Equation 1 stating that $m_{\text{plate}} >> m_{\text{Au}}$ which is likely since $m_{\text{plate}}/m_{\text{Au}} \sim 3$. In order to decrease the discrepancy between the theoretical and measured value either a thinner Au layer or a layer of lower density should be used. In Table 2 the sensitivity normalized to the area of the CMUT cell is also given in order to ease comparisons with other CMUT sensors in the literature.

In order to compare sensitivities of different types of resonant gravimetric sensors a normalized sensitivity should be used. One way of calculating this

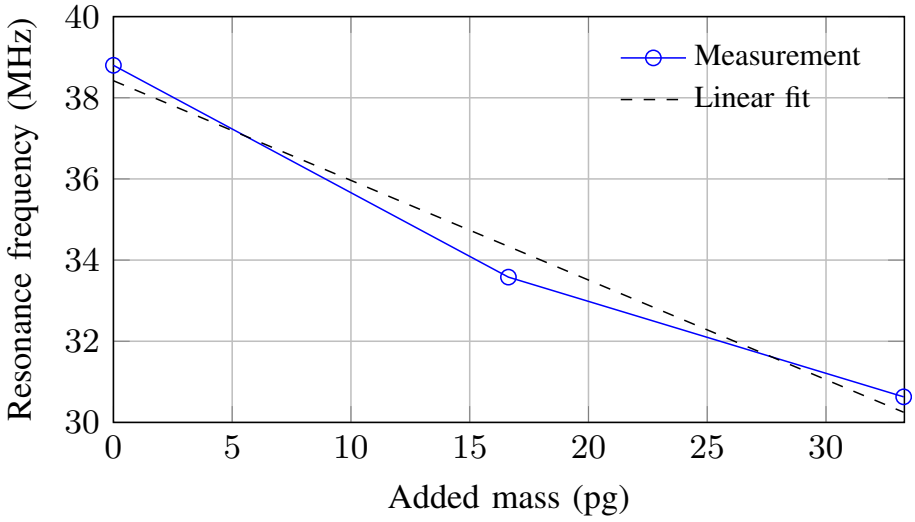


Figure 4: Resonance frequency as a function of added mass from the Au deposition.

normalized sensitivity is given by [15]:

$$S_{\text{norm}} = \lim_{\Delta m \to 0} \frac{1}{f_0} \frac{\Delta f}{\Delta m / A} = \frac{\partial f}{\partial m} \frac{A}{f_0} = \frac{1}{2\rho t}, \tag{2}$$

where $\rho$ and $t$ is the mass density and thickness of the plate, respectively. Equation 2 can be seen as a normalized version of Equation 1 with respect to the area and resonance frequency. For the CMUT the normalized sensitivity only depends on the inverse product of the mass density of the plate material and the thickness of the plate. The normalized sensitivity is therefore maximized, for a given material, by having a thin plate.

### *2.1.4. Limit of detection*

The mass limit of detection (LOD) is a measure of the minimum change in mass a sensor can detect due to frequency noise. The LOD can be estimated by the following relation [2]:

$$\text{LOD}(\tau) = 2m_{\text{eff}}\sigma(\tau), \tag{3}$$

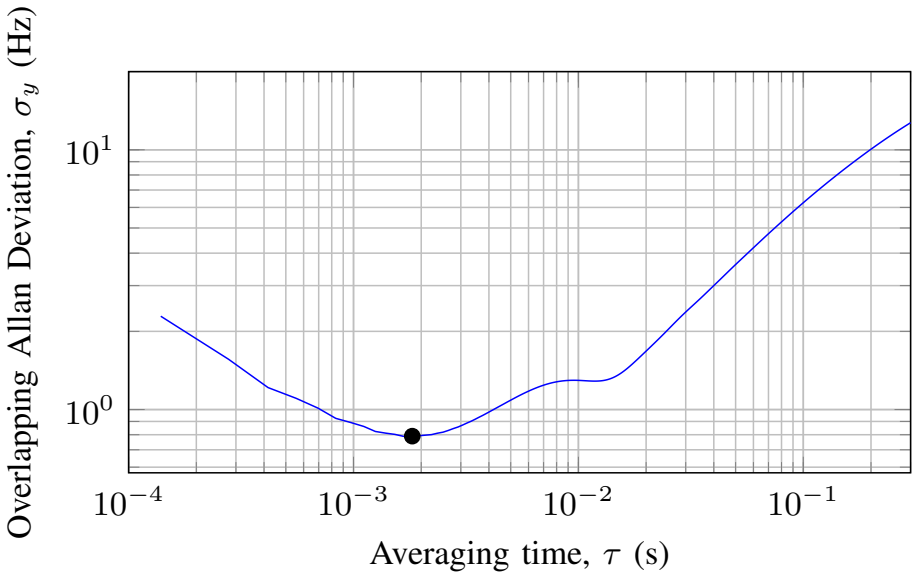


Figure 5: Overlapping Allan deviation $\sigma_y$ as a function of averaging time $\tau$. Phase lock loop band width: 10 kHz.

where $m_{\text{eff}}$ is the effective mass of the plate and $\sigma(\tau)$ is the Allan deviation. The effective mass of the plate is lower than the total geometrical mass ($m_{\text{eff}} < m_{\text{total}} = \rho t A$) but in all calculations in this paper the total geometrical mass has been used in order to follow the established practice. The overlapping Allan deviation is shown in Figure 5 and is calculated from frequency noise data for the CMUT device. The minimum point on the graph is used to calculate the minimum LOD = 2.0 ag, using Equation 3. The results are gathered in Table 2 where also the normalized LOD is included.

### *2.2. Colorimetric chip and functionalization*

The colorimetric arrays consist of two columns of dye spots. The spots in the right column are made of Reichardt's dye (CAS no.: 10081-39-7) [16], here called coating A, and the dye spots in the left column, here called coating B, is Bengal Rose B (CAS no.: 632-69-9) [17]. Coating A has solvatochromic properties where the color changes depending on the polarity of the analyte. This is not

the case for coating B, and coating A is therefore expected to change color when in contact with the least polar molecule: BMK, while coating B is not expected to react. The analytes are physically adsorped on the dyes through Van der Waals interactions, hydrogen bonds, and $\pi$-$\pi$ interactions, all of which are weak interactions. The dye spots are made by dispensing several droplets of dye in a liquid solution on a white polypropylene substrate. The dispensing and spot pattern are controlled by a computer and an automatic dispensing machine (GESIM, Nano-Plotter) using a piezoelectric actuated needle. The same setup is used to coat the CMUT surfaces with dye. The two dyes used for the colorimetric arrays are used as functionalization layers on the CMUTs. The resonance frequency of the CMUTs decreased by approximately 4 MHz, after coating A or coating B was applied. A decrease in resonance frequency is expected as the functionalization layers add mass to the plates.

## 3. Experimental setup

The experimental setup is constructed so the CMUT frequency shift and colorimetric color change can be measured simultaneously. The CMUTs and the colorimetric chip are placed in a small ($\sim 72\,\mathrm{cm}^3$) chamber, see Figure 6a). Through an inlet hole in the chamber, analytes can be injected. The analytes are in the liquid phase when injected into the chamber where they evaporate and thus increase the gas phase concentration of the analyte until the vapour pressure is reached. The CMUT is glued to a Transistor Outline 8 (TO-8) package which functions as a chip carrier. Au wirebonds connect the top and bottom electrodes of the CMUT to two macroscopic pins, see Figure 6b). In addition, a coated CMUT element can be seen in this figure. A microscope records an image of the colorimetric chip every 30 s through the transparent top of the chamber. An example of such an image can be seen in Figure 6c), showing the two columns of dye spots. Finally, the CMUT is connected to a bias tee which supplies the CMUT with a DC voltage (Keithley, 2410) and an AC voltage from a lock-in amplifier with a built-in phase locked loop (Zurich Instruments,

HF2LI PLL), see Figure 6d). The PLL ensures that the CMUT is driven at resonance while the resonance frequency shifts are saved to a computer. The resonance frequency can be measured for two CMUT elements simultaneously.

## 4. Results

The color change of the colorimetric dyes is found by analysing the optical images recorded as time passes. Difference maps are created by subtracting all images from a reference image, which here is chosen as the image at $t = 0\,\mathrm{s}$. The difference maps highlight the *changes* in color and intensity of the dyes. Figure 7a) and b) show two microscope images before and after BMK (99 %, CAS no.: 103-79-7) has reacted with the dyes, respectively. Figure 7c) and d) show the difference maps at the corresponding times, where c) is all black since this was used as the reference image and d) clearly exhibits a color change for dye A.

Figure 8 shows the intensity of the difference maps inside the dye spots A and B as a function of time. The intensity is calculated by taking the mean of the RGB values from the difference map in the area inside the dye spots. The three graphs each shows the intensity as a function of time when either a) BMK, b) acetone or c) deionized water is introduced at $t = 4\,\mathrm{min}$. In Figure 8 a) dye A shows an increase in intensity after BMK is injected and at about $t = 15\,\mathrm{min}$ the intensity has reached a constant maximum value and it is assumed that all the dye has reacted with the BMK. The intensity of dye B does not change as a function of time since no color change has occurred. In addition, no color change is observed, for either coating, when acetone or water is injected, see Figure 8b) and c) respectively. Acetone is chosen as an analyte since the molecular structure is similar to that of BMK expect for an aromatic ring and water is chosen since water vapour is almost always present in the atmosphere in real life applications. Figure 8 demonstrates that coating A has an affinity towards BMK while coating B does not. Furthermore, coating A demonstrates a selectivity between BMK, acetone and water, since no color change is observed for the two latter cases.

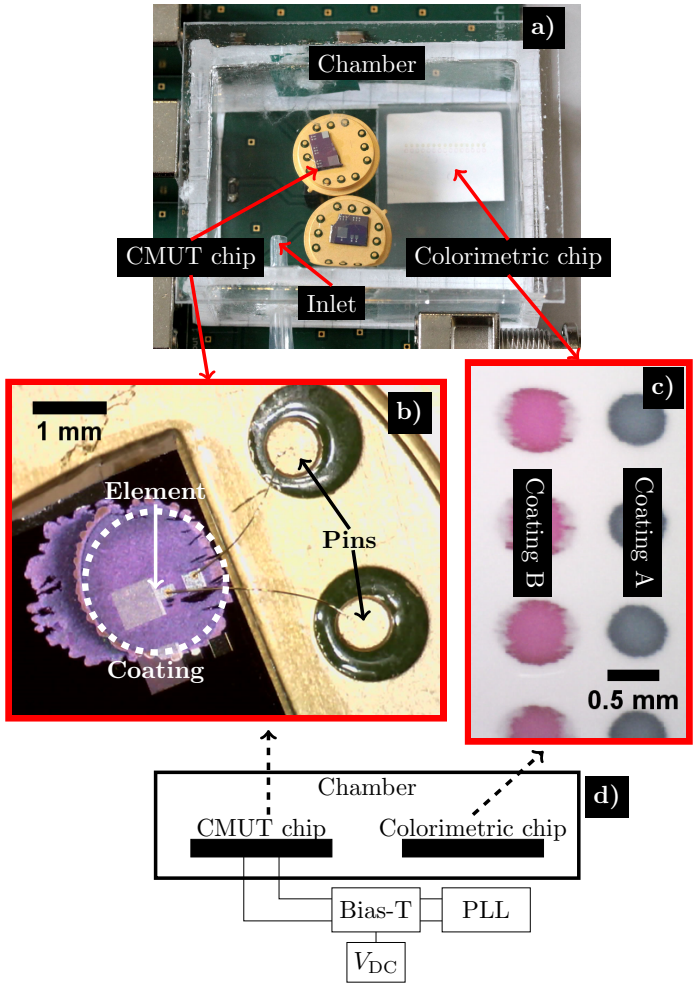


Figure 6: a) Top view photograph of the chamber enclosing the CMUT chips and the colorimetric chip. b) Optical microscope image of the CMUT chip wirebonded to two pins. A single element is seen, coated with dye. c) Optical microscope image of the colorimetric chip showing the two columns of dye spots. d) Schematic cross section of the experimental setup showing the chamber enclosing the CMUT and colorimetric chip. The electrical actuation/readout circuit of the CMUT is also seen which consists of a phase locked loop, a bias tee, and a DC power supply.

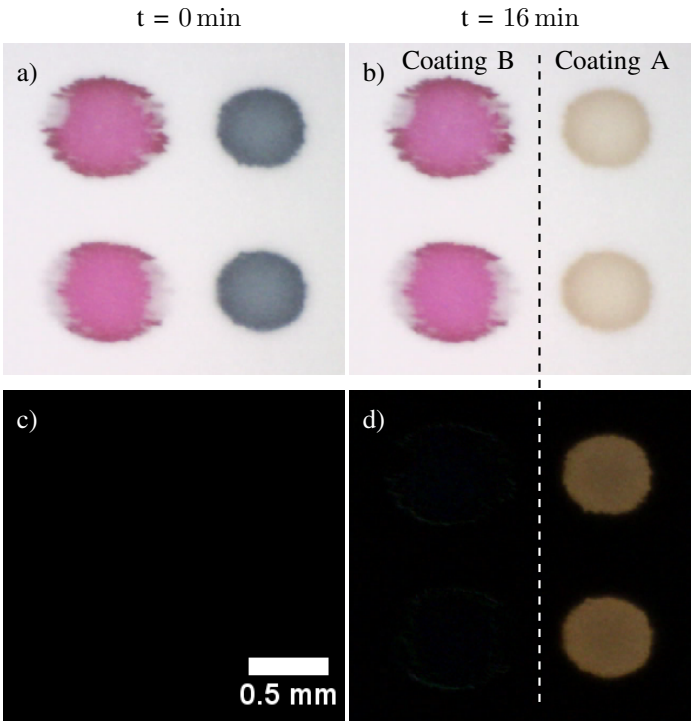


Figure 7: Coating A and B, a) before and b) after reaction with BMK. Difference maps c) before and d) after reaction with BMK. BMK is injected at $t = 4$ min.

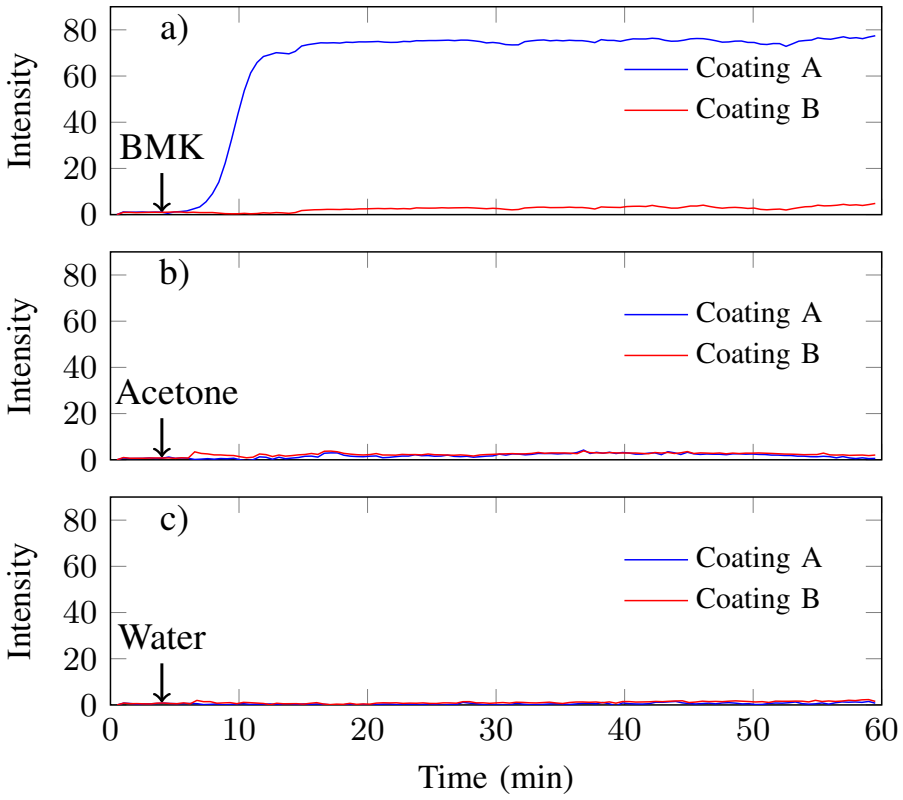


Figure 8: Mean intensity of the red, green and blue channels as a function of time for a) BMK, b) acetone and c) water inside the dye spot area. The analyte is introduced at $t = 4\,\text{min}$ indicated by an arrow.

Figure 9 shows two plots of the frequency shift as a function of time for two CMUTs coated with the two dyes. The added mass on the right axis is calculated using Equation 1 and the measured frequency shift. Two experiments are performed where in Figure 9, a) BMK and b) water are injected into the chamber, respectively. Consequently, the resonance frequency decreases due to the added mass of the evaporated analytes on the plate of the CMUT. The larger decrease in resonance frequency, in Figure 9a), for the CMUT with coating A, demonstrates that coating A has a stronger affinity towards BMK than the CMUT with coating B and no coating. Thus, the largest intensity change is observed for coating A and the largest frequency shift is observed for the CMUT with coating A. In order to test the selectivity of the coatings and whether the difference observed is due to the coatings and not due to differences of the specific CMUTs, the experiment is repeated with water as an analyte, see Figure 9b). The CMUT with coating A shows the smallest frequency shift. Hence, coating A is selective towards BMK both when used as a coating on the CMUTs and when used as a dye in the colorimetric chip.

The difference in the response times between the colorimetric chip and CMUT is due to the fact that for a color change to occur only a monolayer of molecules will saturate the colorimetric response while the gravimetric response is affected by subsequent surface layers and possibly also absorption into the volume of the dye. The CMUT response is therefore not saturated in the same way as the color change of the colorimetric chip, and can continue to show a change in resonance frequency.

## 5. Discussion

Normalized mass sensitivities for different gravimetric sensor types are plotted in Figure 10. The normalized sensitivities in the figure are examples of the state of the art for each sensor type. The plot shows that of the sensor types CMUTs have the second highest normalized sensitivity, with nanoelectromechanical system (NEMS) sensors being the highest, due to the small dimensions

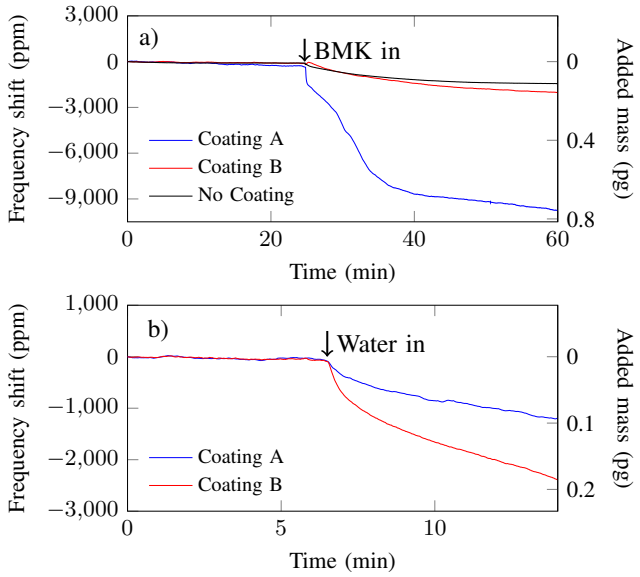


Figure 9: Frequency shift and added mass as a function of time for a) BMK and b) water as analyte.

of these sensors. However, CMUTs are still desirable to use as gravimetric sensors due to a lower LOD [2], a higher SNR and an easier functionalization process. The highest normalized sensitivity of the CMUTs is obtained by the sensor with the thinnest plate, in agreement with Equation 2. This is the device presented in this work which has a plate thickness of 100 nm.

As described in Section 2.1, the CMUT cells were fabricated using a single LOCOS process and wafer fusion bonding to a $Si_3N_4$ plate. CMUTs have previously been fabricated by fusion bonding of $SiO_2$ and $Si_3N_4$ surfaces but the cavities were in these cases made with a reactive ion etch (RIE) process [27, 28]. In [28] a CMP step was required in order to reduce the roughness of the $Si_3N_4$ surface which was not needed in the process used in this paper. This is most likely due to the relatively thin (100 nm) $Si_3N_4$ layer, since a thicker layer typically results in a higher surface roughness which is more difficult to wafer bond [29]. The advantage of using a LPCVD $Si_3N_4$ layer as a plate compared with using the Si device layer of a SOI wafer is a reduced cost and an increased

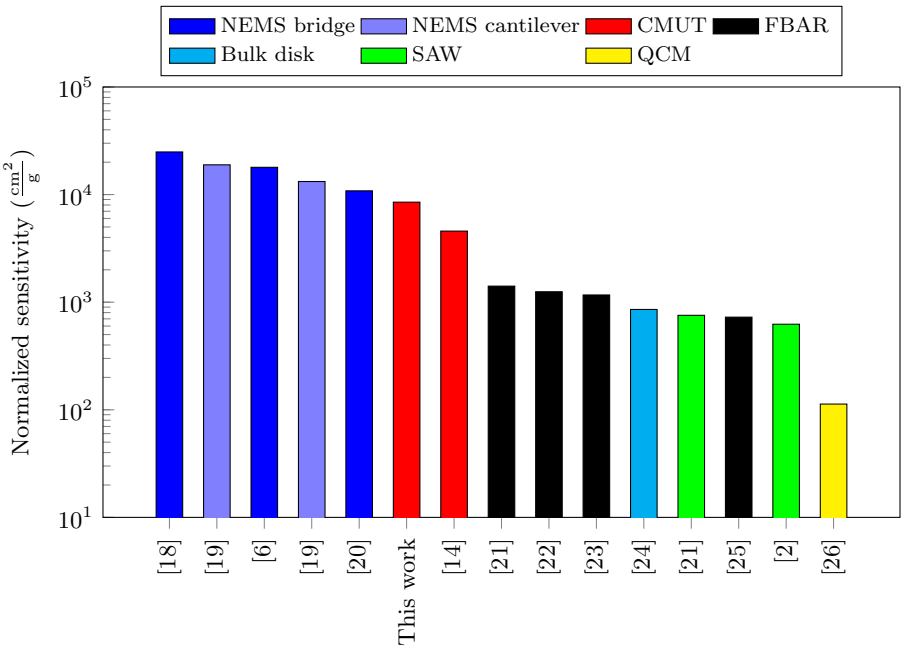


Figure 10: Normalized sensitivity (see Equation 2) for different gravimetric sensor types.

thickness uniformity. In addition, it is difficult to obtain 100 mm SOI wafers with a device layer thinner than a couple hundreds nm, which, in the case of CMUTs for sensing, is desired for increasing the mass sensitivity.

## 6. Conclusion

A sensor system consisting of a CMUT and a colorimetric array was fabricated and used to detect BMK in the gas phase. The CMUT frequency shift directly gave the mass of the absorbed BMK while the colorimetric array demonstrated selectivity between BMK, acetone and water. When used as a functionalization layer on the CMUT, the dye also provided the CMUT with an affinity for BMK, compared with water. The CMUTs were fabricated using a single LOCOS step and wafer bonding to a thin (100 nm) $Si_3N_4$ plate, thus eliminating the need for expensive SOI wafers. Furthermore, the sensitivity of the CMUT was both measured and calculated which resulted in the

lowest sensitivity reported: $28.3\,\frac{\mathrm{zg}}{\mathrm{Hz}\cdot\mu\mathrm{m}^2}$. The normalized sensitivity was found to be $8.5\times10^3\,\frac{\mathrm{cm}^2}{\mathrm{g}}$ which is surpassed only by NEMS cantilevers/bridges when comparing with other resonant gravimetric sensor types, which highlights one of the advantages of using the CMUT as a gravimetric sensor. Future work could include making a setup where the color change is measured for the dye directly on the CMUT chip. Furthermore, it should be investigated whether the dyes can be regenerated e.g. by flushing with an inert gas since the analytes only interact with the dyes through weak interactions.

## References


[1] I. J. Forbes, K. P. Kirkbride, The Origin of Alkenes in Illicit Amphetamine: An Examination of the Illicit Synthesis of Phenyl-2-Propanone, Journal of Forensic Sciences 37 (5) (1992) 1311 – 1318. doi:10.1520/JFS13318J.

[2] S. Fanget, S. Hentz, P. Puget, J. Arcamone, M. Matheron, E. Colinet, P. Andreucci, L. Duraffourg, E. Myers, M. Roukes, Gas sensors based on gravimetric detection - A review, Sensors and Actuators B: Chemical 160 (2011) 804 – 821. doi:10.1016/j.snb.2011.08.066.

[3] S. Munoz-Aguirre, A. Yoshino, T. Nakamoto, T. Moriizumi, Odor approximation of fruit flavors using a QCM odor sensing system, Sensors and Actuators B 123 (2007) 1101 – 1106. doi:10.1016/j.snb.2006.11.025.

[4] M. Zhang, L. Du, Z. Fang, Z. Zhao, A Sensitivity-Enhanced Film Bulk Acoustic Resonator Gas Sensor with an Oscillator Circuit and Its Detection Application, Micromachines 8 (25) (2017) 1 – 11. doi:10.3390/mi8010025.

[5] W. P. Jakubik, Surface acoustic wave-based gas sensors, Thin Solid Films 520 (2011) 986 – 993. doi:10.1016/j.tsf.2011.04.174.

[6] Y. T. Yang, C. Callegari, X. L. Feng, M. L. Roukes, Surface Adsorbate Fluctuations and Noise in Nanoelectromechanical Systems, Nano Lett. 11 (2011) 1753 – 1759. doi:10.1021/nl2003158.

[7] H. J. Lee, K. K. Park, M. Kupnik, Ö. Oralkan, B. T. Khuri-Yakub, Chemical Vapor Detection Using a Capacitive Micromachined Ultrasonic Transducer, Anal. Chem. 83 (2011) 9314 – 9320. doi:10.1021/ac201626b.

[8] K. K. Park, H. J. Lee, G. G. Yaralioglu, A. S. Ergun, Ö. Oralkan, M. Kupnik, C. F. Quate, B. T. Khuri-Yakub, T. Braun, J.-P. Ramseyer, H. P. Lang, M. Hegner, C. Gerber, J. K. Gimzewski, Capacitive micromachined ultrasonic transducers for chemical detection in nitrogen, Applied Physics Letters 91 (2007) 094102–1 – 094102–3. doi:10.1063/1.2776348.

[9] D. Virzonis, G. Vanagas, A. Ramanaviciene, A. Makaraviciute, D. Barauskas, A. Ramanavicius, W. Wen, R. Kodzius, Resonant gravimetric immunosensing based on capacitive micromachined ultrasound transducers, Microchim Acta 181 (2014) 1749 – 1757. doi:10.1007/s00604-014-1244-3.

[10] H. J. Lee, K. K. Park, M. Kupnik, B. T. Khuri-Yakub, Functionalization layers for CO2 sensing using capacitive micromachined ultrasonic transducers, Sensors and Actuators B: Chemical 174 (2012) 87 – 93. doi:10.1016/j.snb.2012.08.025.

[11] D. Barauskas, D. Pelenis, D. Virzonis, J. P. Baltrus, J. Baltrusaitis, Greenhouse Gas Molecule CO2 Detection Using a Capacitive Micromachined Ultrasound Transducer, Anal. Chem. 88 (13) (2016) 6662 – 6665. doi:10.1021/acs.analchem.6b02085.

[12] Q. Stedman, K.-K. Park, B. T. Khuri-Yakub, Distinguishing Chemicals Using CMUT Chemical Sensor Array and Artificial Neural Networks, IEEE International Ultrasonics Symposium Proceedings (2014) 162 – 165doi:10.1109/ULTSYM.2014.0041.

[13] K. K. Park, H. Lee, M. Kupnik, B. T. Khuri-Yakub, Fabrication of capacitive micromachined ultrasonic transducers via local oxidation and direct wafer bonding, Journal of Microelectromechanical Systems 20 (1) (2011) 95–103. doi:10.1109/JMEMS.2010.2093567.

[14] H. J. Lee, K. K. Park, Ömer Oralkan, M. Kupnik, B. T. Khuri-Yakub, A Multichannel Oscillator for a Resonant Chemical Sensor System, IEEE Transactions on Industrial Electronics 61 (10) (2014) 5632 – 5640. doi:10.1109/TIE.2014.2300031.

[15] S. W. Wenzel, R. M. White, Analytic comparison of the sensitivities of bulk-wave, surface-wave, and flexural platewave ultrasonic gravimetric sensors, Appl. Phys. Lett. 54 (1989) 1976 – 1978. doi:10.1063/1.101189.

[16] C. Machado, V. G. Machado, An easy and versatile experiment to demonstrate solvent polarity using solvatochromic dyes, Journal of Chemical Education 78 (5) (2001) 649–651. doi:10.1021/ed078p649.

[17] L. Ludvíková, P. Friš, D. Heger, P. Šebej, J. Wirz, P. Klán, Photochemistry of rose bengal in water and acetonitrile: a comprehensive kinetic analysis, Phys. Chem. Chem. Phys. 18 (2016) 16266–16273. doi:10.1039/C6CP01710J.

[18] Y. T. Yang, C. Callegari, X. L. Feng, K. L. Ekinci, M. L. Roukes, Zeptogram-Scale Nanomechanical Mass Sensing, Nano Lett. 6 (4) (2006) 583 – 586. doi:10.1021/nl052134m.

[19] M. Li, H. X. Tang, M. L. Roukes, Ultra-sensitive NEMS-based cantilevers for sensing, scanned probe and very high-frequency applications, Nature Nanotechnology 2 (2007) 114 – 120. doi:10.1038/nnano.2006.208.

[20] K. L. Ekinci, M. L. Roukes, Nanoelectromechanical systems, Rev. Sci. Instrum. 76 (2005) 061101–1 – 061101–12. doi:10.1063/1.1927327.

[21] G. Wingqvist, L. Arapan, V. Yantchev, I. Katardjiev, A micromachined thermally compensated thin film Lamb wave resonator for frequency control and sensing applications, J. Micromech. Microeng. 19 (2009) 1 – 9. doi:10.1088/0960-1317/19/3/035018.

[22] J. Weber, W. M. Albers, J. Tuppurainen, M. Link, R. Gabl, W. Wersing, M. Schreiter, Shear mode FBARs as highly sensitive liquid biosensors, Sensors and Actuators A 128 (2006) 84 – 88. doi:10.1016/j.sna.2006.01.005.

[23] Y. Feng, M. Liu, X. Li, J. Li, Micromachined mass sensor based on film bulk acoustic resonator, Symposium on Piezoelectricity, Acoustic Waves, and Device Applications (2015) 228 – 231doi:10.1109/SPAWDA.2015.7364478.

[24] A. Cagliani, Z. J. Davis, Ultrasensitive bulk disk microresonator-based sensor for distributed mass sensing, J. Micromech. Microeng. 21 (2011) 1 – 6. doi:10.1088/0960-1317/21/4/045016.

[25] H. Zhang, E. S. Kim, Micromachined Acoustic Resonant Mass Sensor, Journal of Microelectromechanical Systems 14 (4) (2005) 699 – 706. doi:10.1109/JMEMS.2005.845405.

[26] M. Pohanka, The Piezoelectric Biosensors: Principles and Applications, a Review, Int. J. Electrochem. Sci. 12 (2017) 496 – 506. doi:10.20964/2017.01.44.

[27] K. Midtbø, A. Rønnekleiv, D. T. Wang, Fabrication and Characterization of CMUTs realized by Wafer Bonding, IEEE Ultrasonics Symposium (2006) 934 – 937doi:10.1109/ULTSYM.2006.249.

[28] A. I. H. Chen, L. L. P. Wong, Z. Li, S. Na, J. T. W. Yeow, Practical CMUT Fabrication With a Nitride-to-Oxide-Based Wafer Bonding Process, Journal of Microelectromechanical Systems 26 (4) (2017) 829 – 836. doi:10.1109/JMEMS.2017.2675987.

[29] K. Reck, C. Østergaard, E. V. Thomsen, O. Hansen, Fusion bonding of silicon nitride surfaces, J. Micromech. Microeng. 21 (2011) 1–5. doi:10.1088/0960-1317/21/12/125015.